Journal of the European Ceramic Society 43 (2023) 2752–2760

Contents lists available at ScienceDirect

Journal of the European Ceramic Society

journal homepage: www.elsevier.com/locate/jeurceramsoc

# Material extrusion additive manufacturing of advanced ceramics: Towards the production of large components

Frank Clemens [a,*], Fateme Sarraf [a,b], Aurelio Borzì [c], Antonia Neels [c], Amir Hadian [a]

[a] Laboratory for High Performance Ceramics, Empa-Swiss Federal Laboratories for Materials Science and Technology, Ueberlandstrasse 129, CH-8600 Dübendorf, Switzerland
[b] University of Bern, Hochschulstrasse 6, CH-3012 Bern, Switzerland
[c] Center for X-ray Analytics, Swiss Federal Laboratories for Material Science and Technology, Empa, Überlandstrasse 129, CH-8600 Dübendorf, Switzerland

ARTICLE INFO

*Keywords:*
Material extrusion (MEX) additive manufacturing
Fused deposition modeling (FDM)
Fused filament fabrication (FFF)
YSZ
$ZrO_2$

ABSTRACT

Thermoplastic extrusion based additive manufacturing (MEX-AM), is a very interesting fabrication method for the shaping of larger ceramic parts. Commercial filaments are currently available in the market, but due to the lack of information from the suppliers, it is not easy to select the suitable filament material for the 3D printing of individual ceramic objects. In this study, three commercial yttria-stabilized zirconia (YSZ) filaments provided by Fabru GmbH, SiCeram GmbH and PT+A GmbH were investigated. According to our results, it is possible to print YSZ filaments with extremely different flexibility and rheological properties. Compared to the other two filaments, the Fabru filament resulted in significantly higher flexibility, but the extrusion pressure to print it through a 0.25 mm nozzle was significantly higher at 150 °C. Interestingly, in the SiCeram filament, a grain orientation effect could be observed. Based on STA analysis it can be assumed that for the Fabru filament, the polymer which decomposes at a high temperature can already be removed by solvent debinding (SD). Finally, 70 mm tall cup structure including overhang features and different wall thicknesses was used to evaluate the printing and post-processing of YSZ filaments.

## 1. Introduction

Additive manufacturing (AM) of ceramic structures became very popular in the last decade. In contrast to subtraction processing methods, the structure is built up layer-by-layer. According to ASTM F2792 [1], additive manufacturing processes can be categorized into seven groups. Among others, material extrusion based additive manufacturing (MEX-AM) is an established method for the fabrication of macroscopic commercial products [2].

Unfortunately, different names have been given for similar fabrication methods. From the mid-90 s till the beginning of the 21st century, researchers called the process fused deposition of ceramics (FDC) to highlight the post-processing by thermal debinding of the thermoplastic binder and the sintering of the ceramic after the 3D printing step [2–12]. Later the name FDC disappeared from the literature, and is used again today by some scientists [13,14].

To highlight that the Bowden extruder head was replaced by a screw extruder, Bellini et al. [12] renamed the process using the term mini extruder deposition (MED) in 2005, while others used the name composite extrusion modeling (CEM) [15], fused feedstock deposition (FFD) [16] and fused deposition modeling (FDM) [17,18]. Unfortunately, the same name, FDM, was used for filament based extruder heads (e.g. Bowden and direct drive extruder heads) too [19–23]. To make the naming even more complicated. since 2019 researchers started to use the name fused filament fabrication (FFF) when they used ceramic filaments for the 3D printing process [24–37].

Due to the naming issue, mentioned above, in some journals, researchers are encouraged to use the name material extrusion based additive manufacturing [38–43], as suggested by the ASTM F2792 [1]. Therefore, Rane et al. [43] and Hadian et al. [44] used the name extrusion based additive manufacturing for the printing with screw extruder heads too.

Different ceramic materials, like hydroxyapatite $Ca_5(PO_4)_3(OH)$, aluminium oxide ($Al_2O_3$), zirconium oxide ($ZrO_2$), aluminium oxide toughened zirconium oxide (ATZ), lead zirconate titanate (PZT), barium titanate ($BaTiO_3$), preceramic polymers (PCP), silicon carbide (SiC) as well as silicon nitride ($Si_3N_4$), have been investigated for the thermoplastic based material extrusion based additive manufacturing (MEX-

* Corresponding author.
*E-mail address:* frank.clemens@empa.ch (F. Clemens).

https://doi.org/10.1016/j.jeurceramsoc.2022.10.019
Received 30 June 2022; Received in revised form 7 October 2022; Accepted 11 October 2022
Available online 13 October 2022

AM) and a good overview has been reported by Clemens et al. [2]. In 2022 Freudenberg at al. [36] and Abel et al. [37] have been started to investigate non-oxide ceramic matrix composite filaments for the thermoplastic MEX-AM process.

Compared to other ceramic AM processes, MEX-AM benefits from a fast and simple 3D printing process with low investment costs to achieve strong green parts. Therefore, MEX-AM process is interesting to build up larger ceramic structures. Additionally, it is possible to fabricate multi-material components or functionally graded materials using multi-head printers. The reason that thermoplastic binder additive are used, printed filament material can be recycled and this lows the material waste production during the fabrication process [44].

However, lower resolution in comparison to VAT polymerization AM and long post-processing cycles (i.e. binder removal and sintering) will be a challenging task for small and large components, respectively.

Commercial ceramic filaments like YSZ and $Al_2O_3$ are already available [35]. YSZ filaments have received higher attention due to the high toughness and mechanical strength of zirconia. As demonstrated by Hadian et al. [40], MEX-AM can be used to print and sinter large (e.g. 12 cm tall) zirconia vase structures successfully. Recently, Hadian et al. [44] investigated the mechanical strength of dense YSZ discs manufactured by MEX-AM process using a commercial filament. In addition, they made their feedstock using commercial thermoplastic binders that were developed for ceramic injection molding. Because of the different material properties, different printing heads had to be used for the shaping process. To find the right printing parameters, several test prints had to be done because of the lack of information given by the supplier for the ceramic filament. It will be of great interest to have more data from the filament material to be able to select the suitable material and printing parameters more easily for the 3D printing of individual ceramic objects.

Inspired by the results of Hadian et al. [40,43], in this study three different commercial YSZ filaments, namely SiCeram GmbH, PT+A GmbH and Farbu GmbH to fabricate large ceramic objects, were investigated. Filament properties like flexibility, extrusion pressure, post-processing, e.g. the debinding and sintering, phase composition as well as grain orientation and the viscosity were analyzed. Later the filament results were compared with the results achieved by printing of large objects.

## 2. Material and methods

### 2.1. Materials and printing design

In this study, commercial YSZ filaments of SiCeram GmbH (SiCeram), PT+A GmbH (PT+A) and Fabru GmbH (Fabru) with a diameter of 1.75 mm were used for the printing of a cup as shown in Fig. 1.

The cup design (open source, grabcad community) was selected to investigate the printing and post-processing behavior of an overhang structure with different wall thicknesses. In the cup design, the wall thickness varies from 4 to 14 mm which can result in different solvent debinding behavior and deformation during the thermal treatments.

### 2.2. Characterization of the commercial YSZ filaments

To investigate the as-received YSZ filaments from the different suppliers, the density of the filaments was analyzed by He-pycnometer (Ultrapyc 500, Anton Paar GmbH, Austria) and the filament diameter was measured with a caliper. The flexibility of filaments was evaluated as the minimum bending radius to which a filament could be bent before it fractured.

Elemental analysis was performed on the fracture surface of the filaments using a scanning electron microscope (VEGA3, TESCAN Co., Czech Republic) equipped with an energy dispersive spectrometer (EDS, Xflash 610, Bruker Nano GmbH, Germany). To avoid surface charging by the incident electron beam, a 25 nm carbon coating was applied by a high vacuum sputter (EM ACE200, Leica Microsystems, Austria). Parameters for EDS analysis were kept constant for all samples (e.g. magnification of 1000 x and accelerating voltage 10 kV).

To investigate the homogeneity of the YSZ filaments, Rosand RH7 capillary rheometer (Flowmaster, Netzsch GmbH, Germany) was used. A constant mass of 140 g was filled in the bore and heated up to 150 °C. Using a customized adapter, an E3D V6 nozzle with a diameter of 0.25 mm was fixed on the bottom of the rheometer and the tests were performed with a constant shear rate of 6′000 $s^{-1}$. It is worthwhile to mention that due to the different densities of the commercial filaments the time of the test slightly varied.

The binder removal and sintering were investigated on the three commercial filaments after the solvent debinding and after the sintering. The solvent debinding was performed in an acetone bath at room temperature for 48 h for all filaments. After the solvent debinding, the samples were debound and sintered with two different programs. The data sheet of PT+A GmbH recommends a slow debinding between 280 and 650 °C and sintering between 1380 and 1500 °C. SiCeram GmbH and Fabru GmbH provide a debinding and sintering program for the 3D printed parts. SiCeram and Fabru recommend a sintering temperature of 1475 and 1400 °C, respectively. Accordingly, the SiCeram and PT+A debound samples were heated at 4 K/min up to 1000 °C in static air condition. Then, a lower heating rate of 2 K/min was used to reach to 1475 °C in which the samples sintered for 2 h. For the Fabru debound

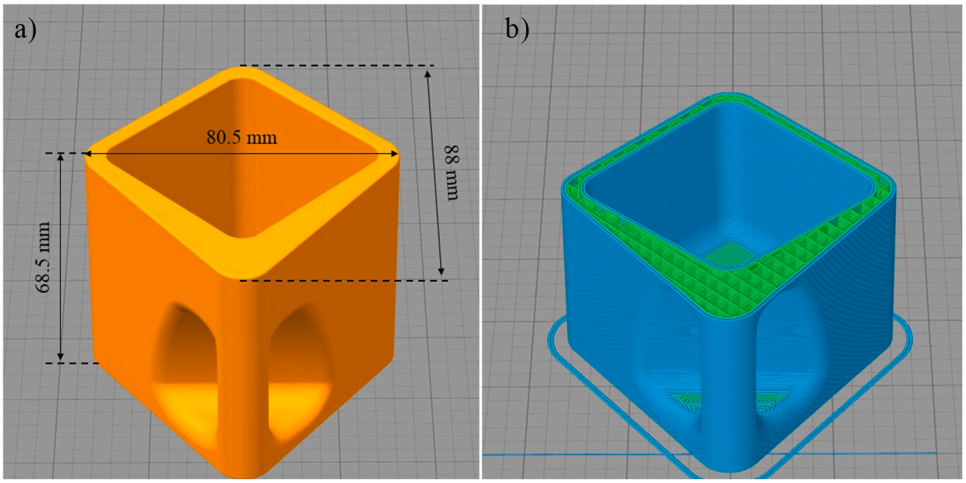


**Fig. 1.** a) 3D model and b) infill pattern of the cup that had to be printed using commercial YSZ filaments.

samples, a heating rate of 3 K/min was used to reach to 1300 °C then the heating rate was raised to 3 k/min to the sintering temperature. In comparison to SiCeram and PT+A, the Fabru samples were sintered at a lower temperature (1400 °C) for a longer period (4 h). Based on the simultaneous thermal analysis (STA) analysis performed on the three different filaments, the same debinding and sintering program for the SiCeram and PT+A filaments was used.

For the different YSZ filaments the thermal binder decomposition with and without the solvent debinding step were investigated with a STA instrument (Jupiter F3 STA 449, Netzsch, Germany). For these experiments, a constant heating rate of 5 K/min and a synthetic air flow rate of 70 ml/min were used. Finally from the analysis, the total mass loss, the onset, and the offset temperatures were investigated. The results were compared with the previous test performed on filaments (e.g. mass loss after solvent debinding and sintering using a balance).

After sintering, x-ray diffraction (XRD) was performed on the polished surface of the filaments. The sintered filaments were embedded in a resin matrix (Epoxy Resin HT 2 + Hardener HT 2, R&G Faserverbundwerkstoffe GmbH, Germany) and the surface was ground and polished (Tegramin-30, Struers, Denmark). XRD patterns were measured with a Malvern Panalytical Empyrean instrument (Netherlands), equipped with Cu-Kα radiation ($\lambda = 1.5418$ Å) and optics at the incident and diffracted beam paths. The size of the beam spot was limited to $1.5 \times 1.0$ mm$^2$ in order to increase the diffraction component of the sample and limit the amorphous background. Radial $\theta/2\theta$ measurements in the range 10–120° have been performed. The angular resolution related to the exploited instrumental setup is 0.05°. The software HighScore Plus (Malvern Panalytical Empyrean instrument, Netherlands) and TOPAS (Bruker Corporation, Switzerland) were used for data treatment and analysis.

To analyze the flow behavior of the three different thermoplastic YSZ materials a rotational viscometer (MCR 302, Anton Paar, Austria) was used. A plate-plate configuration with a disc diameter of 10 mm was used and the distance between the two plates was gradually reduced until a gap size of 1 mm was achieved. Results at higher shear rates were unreliable because the material was expelled from the fixed gap between the plates.

Due to the different printing temperatures recommended by the different suppliers, the rheological behavior was investigated at three different temperatures. For the SiCeram and PT+A YSZ filaments the rheological behavior was analyzed at 120, 140 and 160 °C. For the Fabru filaments, a temperature of 140, 160 and 180 °C was selected for the rheological investigations.

### 2.3. 3D printing and post-treatment of the commercial YSZ filaments

For the printing of the open source cup design, an Ender 5 Pro (Creality, China) was used. Based on the shrinkage value from the filament analysis, the size of the printed samples were adjusted to achieve the right dimensions after sintering. To get a better printing performance the original print head was replaced by a Hemera direct kit (E3D, England). For the printing, a nozzle with a diameter of 0.6 mm and a speed of 30 mm/s were used. All selected filaments were printed with a constant layer height of 0.2 mm and a constant extrusion width of 0.75 mm. Other optimized printing parameters are reported in the result part later, for the selected filaments.

After the printing, the samples were immersed in an acetone bath for 24 and 48 h. After the solvent debinding, the samples that did not show structural defects (e.g. cracks) were further processed with the thermal treatment (e.g. debinding and sintering program), given by the supplier. Weight loss was evaluated after each processing step. The shrinkage was calculated after the sintering step.

## 3. Results and discussion

### 3.1. Characterization of the commercial filaments

After receiving the commercial filaments, the density, diameter and flexibility (i.e. the minimum bending radius before fracture) were investigated. Table 1 shows the results including the received density (supplier information) of the ceramic after sintering as reported by the data sheet of the suppliers.

The main significant difference in Table 1 is the bending radius before fracture and the slightly higher printing temperature given by Fabru GmbH. The two YSZ filaments of the suppliers SiCeram and PT+A show a significantly higher bending radius in comparison to the Fabru YSZ filament.

The main components of the filaments were identified by EDS analysis presented in Fig. 2. All samples contain Zr, Y, O, Hf, and C. The presence of Zr, Y, and O confirms the use of yttria-stabilized zirconia (YSZ) powder as the filler for all commercial filaments. The intense carbon peak in all samples is due to the thermoplastic binder and the carbon coating used for charge removal. All samples contain a low amount of hafnium. This can be explained by the extreme chemical similarity of hafnium and zirconium which makes the complete separation of these elements difficult in the refining process [45]. For the SiCeram filament an additional peak related to Al could be detected in the magnified view presented in Fig. 2 inset. The presence of minor Al impurity (e.g. 0.25 wt%) in commercial zirconia dental implants was shown by Gross et al. [46].

A homogeneity analysis was investigated with a 0.25 mm E3D V6 nozzle and a capillary rheometer. To be able to compare the three different YSZ filaments a constant temperature (150 °C) and a constant shear rate (6′000 1 $s^{-1}$) were used ( Fig. 3) In comparison to the SiCeram and PT+A YSZ filaments, a much higher extrusion pressure is needed to push the Fabru YSZ filament through the 0.25 mm nozzle. Based on the higher shrinkage and the higher mass loss of the Fabru YSZ filament, which will be discussed in the coming sections, it can be assumed that the different binder recipes will be one of the main reasons for the higher pressure.

The pressure peaks in the flow analysis of the SiCeram and Fabru YSZ filament indicate agglomerates. It seems that the pressure peaks for Fabru YSZ filament are higher, however, a relative peak height of 10% could be calculated for both filaments. Interestingly, for the PT+A filament no agglomerates could be detected during the homogeneity analysis. To further discuss this, it would be important to know if the agglomerates are related to the ceramic powder sources or only to the processing conditions during compounding and filament production. The SiCeram YSZ material resulted in the lowest extrusion pressure and the Fabru material shows the highest extrusion pressure. For the Fabru material, a continuous pressure drop over the extrusion time could be detected. It can be assumed that this is due to the sticking of the melted feedstock on the metal wall of the capillary rheometer bore. When the homogeneity test gets started, the capillary rheometer was filled with a constant mass (140 g). During the test, the bore of the capillary rheometer gets empty meaning the interaction with the wall gets lower, which is in good agreement with the lower piston force values, as can be observed in Fig. 3b.

**Table 1**
Characterization of the three as-received YSZ filaments.

| | SiCeram GmbH | PT+A GmbH | Fabru GmbH |
|---|---|---|---|
| Density Filament [g/ccm] | 3.52 ± 0.01 | 3.52 ± 0.01 | 3.20 ± 0.01 |
| Filament diamenter [mm] | 1.75 ± 0.05 | 1.75 ± 0.05 | 1.75 ± 0.05 |
| Bending radius [mm] | 60 ± 5 | 60 ± 5 | < 16 |
| [a]Density of YSZ [g/ccm] | 6.05 | 6.05 | 6.05 |
| [a]Printing temperature [°C] | 155 – 170 | 130 – 160 | 180–200 |
| [a]Printing speed [mm/s] | 5 – 30 | 30 – 80 | 10–30 |

[a] Datasheet from the supplier

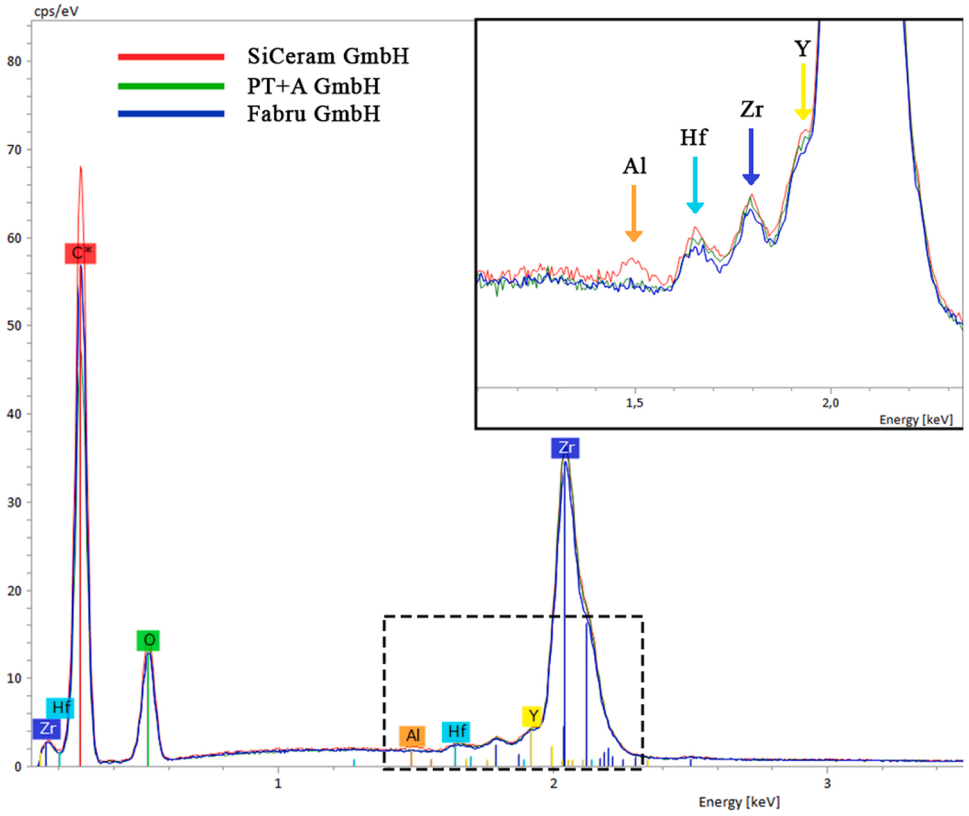


**Fig. 2.** Elemental analysis of three commercial YSZ filaments obtained from energy dispersive X-ray spectroscopy at 10 kV.

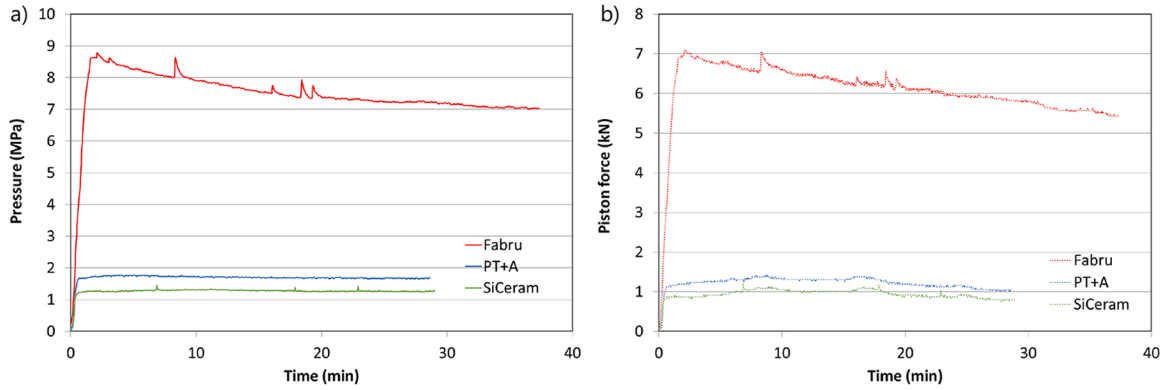


**Fig. 3.** Homogeneity analysis at 150 °C of the three different YSZ filaments (SiCeram, PT+A, and Fabru) using E3D V6 nozzle with a diameter of 0.25 mm and a shear rate of 6′000 $s^{-1-1}$; a) shows the pressure at the die entrance vs. time and b) shows the piston force vs. time.

In addition to the homogeneity tests, debinding and sintering analyses were done for all three YSZ filaments, according to the suppliers. The relative change in mass and diameter was calculated by the difference in mass and diameter between the different processing steps divided by the initial mass and diameter of the filaments, respectively. The results are shown in Fig. 4.

For all filaments, solvent debinding in an acetone bath was recommended by the suppliers. For better comparison, all 1.75 mm filaments were immersed in an acetone bath for 48 h at room temperature. In comparison to SiCeram and PT+A, the Fabru YSZ filament has a lower mass loss. 58 wt% of the total binder remains after the solvent debinding, whereas only 36 and 39 wt% binder needs to burnout after solvent debinding for SiCeram and PT+A, respectively. The total mass loss after sintering is significantly higher for the Farbu YSZ filament, and due to the higher shrinkage, it can be expected that the ceramic powder content is lower compared to SiCeram and PT+A YSZ filaments.

To investigate the thermal decomposition of the thermoplastic binder, STA analysis was performed on YSZ filaments before and after solvent debinding. The results are summarized in Fig. 5.

The total mass loss of the Fabru filament is higher in comparison to the two other ones, as expected in Fig. 4. In the TG (thermogravimetric) experiment, all samples show a different mass loss after solvent debinding (SD) in comparison to Fig. 4. This is due to some residual binder after the solvent debinding step which decomposes during the thermal analysis resulting in a higher total mass loss during thermal analysis of the solvent debound samples. As this difference is around 10%, it can be concluded that 90% of the dissolvable binder was removed during SD step. For the Fabru filament, the DTA (differential thermal analysis) signal at high temperature disappeared after the solvent debinding step. This can be explained by the removal of the

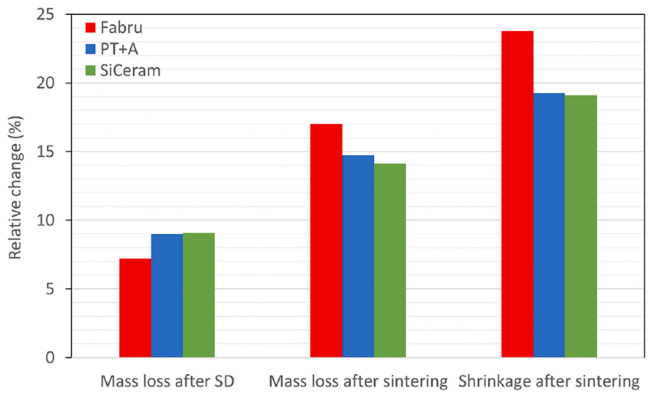


**Fig. 4.** Mass loss and shrinkage analysis of the three different YSZ filaments (SiCeram, PT+A, and Fabru). The mass loss after solvent debinding (SD), after sintering as well as the diameter shrinkage after sintering was investigated.

thermoplastic binder components with high molecular weight during the solvent debinding process.

Finally, the sintered YSZ filaments were investigated by XRD. Due to the small diameter, the samples were embedded in a resin matrix and polished before testing. Fig. 6 shows the XRD pattern of the three filaments and the refinement to investigate the tetragonal and cubic phase composition and grain orientation of the YSZ filament. A list of XRD peaks is provided in the supplementary section (Table S1). Unfortunately, due to the amorphous background of the resin matrix, it was not possible to investigate the monoclinic phase.

XRD patterns do not show a noticeable shift compared to the expected positions, which means that samples are not affected by strain and stress. The broad humps around 20° and 45° relate to the contribution from the amorphous epoxy matrix, used to embed the filaments. Because of these broad humps, monoclinic phase could not be detected. The SiCeram filament shows a higher ratio between the tetragonal and cubic phases, equal to 25 ( ± 12)%. The amount of tetragonal phase decreases in samples PT+A and Fabru, being the ratio equal to 18 ( ± 10)% and 10 ( ± 6)%, respectively.

The XRD pattern of the SiCeram filament shows sharper reflections, which means the sample is more crystalline than PT+A and Fabru. A second difference is related to the orientation of the cubic phase; SiCeram has a remarkable preferential growth along the [110] crystalline direction, with the intensity of the 220 reflection at 49.79° higher than the 111 at 29.85°. PT+A and Fabru do not show preferential orientation.

Finally, the flow behavior of the three different YSZ filaments was investigated by plate-plate rotational rheometer configuration and compared in Fig. 7.

All YSZ filaments show a shear-thinning behavior and as expected, the viscosity decrease by increasing the temperature. For the SiCeram and PT+A filaments, a sharp drop of the viscosity close to a shear rate of 1 $s^{-1}$ was observed. This can be explained by the material flow out of the gap. Due to this reason, the equipment will detect a lower torque which will result in an underestimation of the viscosity.

As shown in Fig. 7a, the viscosity of the Fabru filament was similar at 180 and 200 °C. As mentioned above, for the Fabru filaments, the onset temperature for the binder decomposition starts at 193 °C (Table 2). Due to the binder decomposition, the viscosity will increase and the typical Arrhenius behavior (e.g. lower viscosity at a higher temperature) of

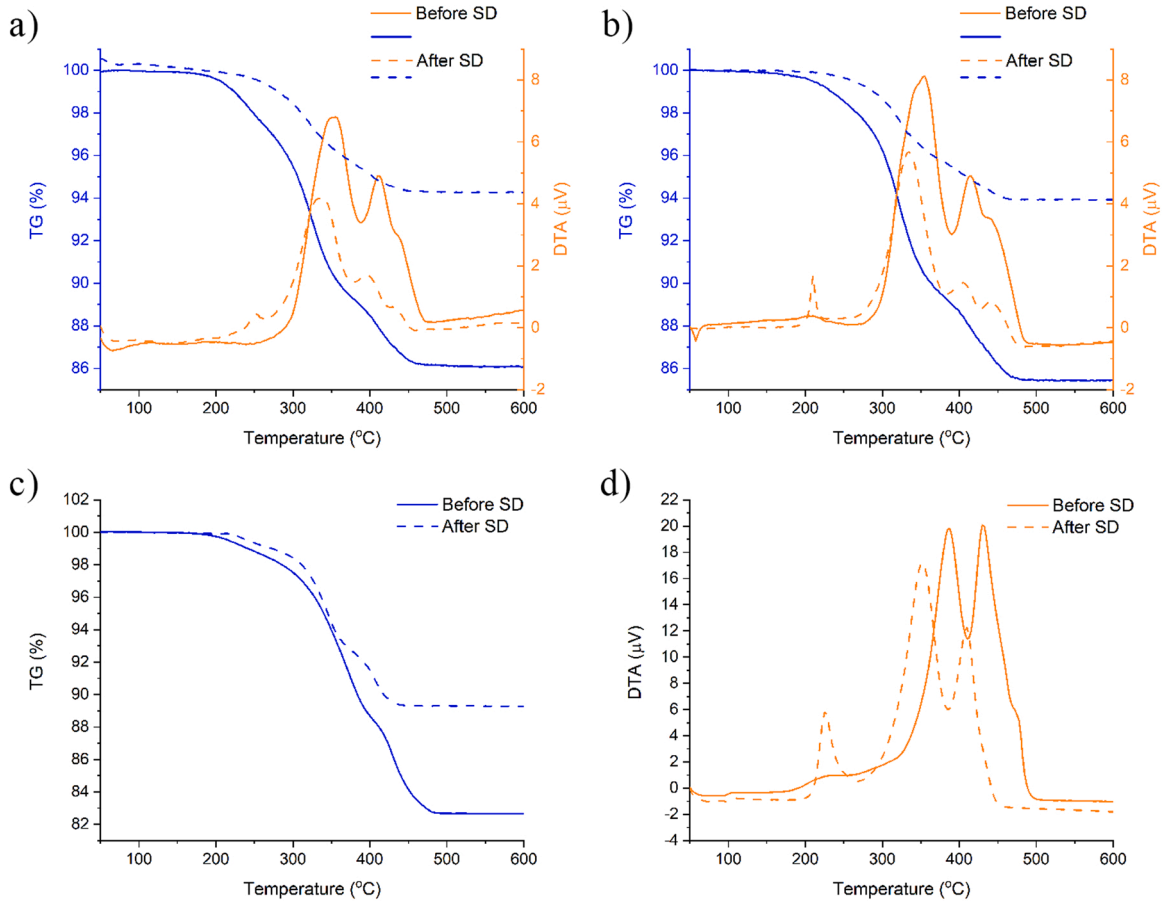


**Fig. 5.** STA analysis of the three different YSZ filaments (SiCeram, PT+A, and Fabru) before and after solvent debinding; a) shows the STA signal of the SiCeram, b) PT+A,c) TG signal, and d) DTA signal for Fabru filaments.

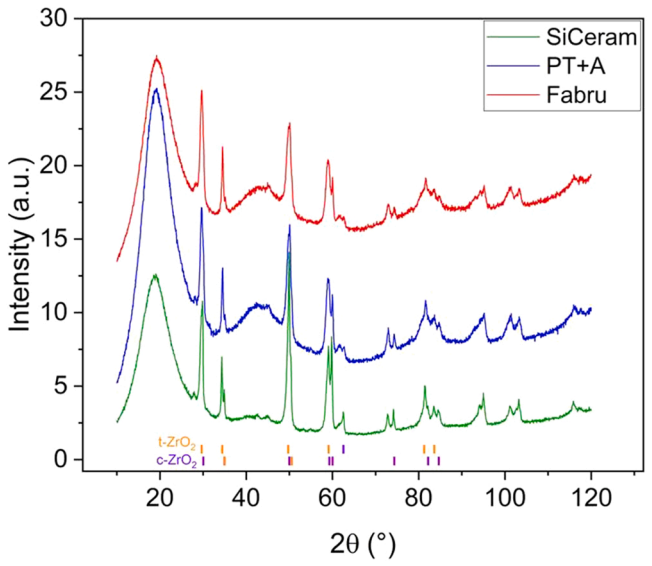


**Fig. 6.** XRD patterns of the sintered filaments. Measurements have been performed on the polished face of the filaments, embedded in a polymer matrix. Broad humps around 20° and 45° are due to the amorphous polymer contribution. Orange and violet lines represent the positions of the XRD peaks for the cubic and tetragonal YSZ phases, respectively. (green) SiCeram; (blue) PT+A; (red) Fabru.

thermoplastic material is not visible anymore.

Fig. 7d shows the comparison of the three different YSZ filaments at 160 °C. The results confirm the pressure analysis of the homogeneity tests investigated with a 0.25 mm E3D V6 nozzle and a capillary rheometer. Therefore, the Fabru filament resulted in higher viscosity, in comparison to the two others. As shown in Fig. 7d the SiCeram has a higher slope, which is equivalent to a higher shear thinning behavior. Therefore at higher shear rates, the SiCeram filaments will result in a lower viscosity in comparison to the PT+A. This explains why the extrusion pressure was lower for the homogeneity tests at a shear rate of 6′000 $s^{-1}$, as shown in Fig. 3.

Based on all results, it can be assumed that the SiCeram and PT+A filaments result in similar behavior. Especially the STA experiments indicated that mass loss onset and offset temperature are similar for two YSZ filaments. In addition, it has to be mentioned that for SiCeram and Fabru filaments, the debinding and sintering parameters are available, whereas in the datasheet of the PT+A YSZ filament only temperature windows are given. Accordingly, for further printing evaluations, SiCeram and Fabru filaments were selected to print cups (Fig. 1).

### 3.2. Printing and post-treatment of the ceramic cup

To print the ceramic cup using SiCeram and Fabru YSZ filaments, the printing parameters had to be optimized to be able to print the structure in a good quality. The optimized printing parameters are presented in Table 3.

For the SiCeram filament a slightly lower extrusion multiplier had to be used to achieve good printing properties. Due to the higher viscosity, the YSZ filament of Fabru had to be printed with a higher nozzle temperature in comparison to the SiCeram one. As seen in Fig. 7, by increasing the melt temperature of the YSZ feedstock, its viscosity decreases. Therefore the difference in viscosity during printing for the two

**Table 2**
Summary of the thermal analysis extracted from Fig. 5.

| | SiCeram | PT+A | Fabru |
|---|---|---|---|
| Mass loss TG [%] | 14 / 6 | 14.5 / 6.1 | 18.2 / 11.8 |
| Mass lossFig. 4 [%] | 14.1 / 9.1 | 14.7 / 9 | 17 / 7.2 |
| Onset temperature [°C] | 191 / 239 | 192 / 231 | 192 / 222 |
| Offset temperature [°C] | 460 / 441 | 477 / 462 | 491 / 438 |

* / * = value before / value after SD

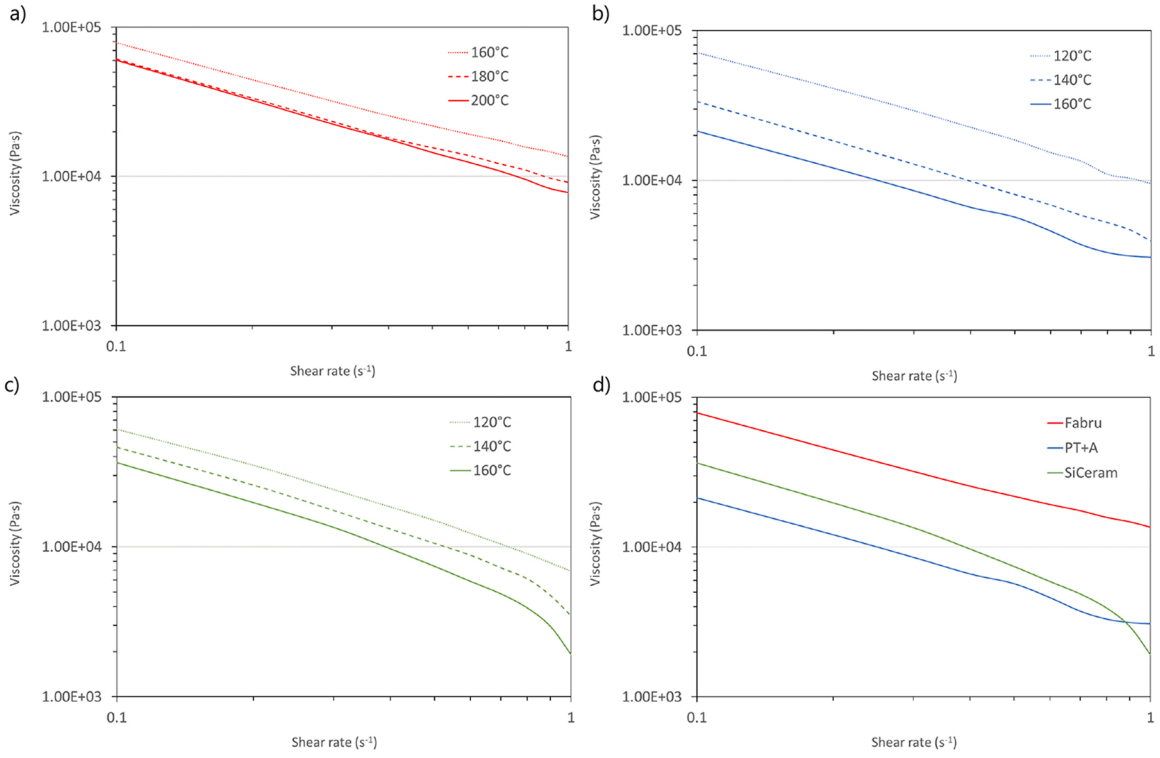


**Fig. 7.** Rheological analysis for the three YSZ filaments at different temperatures, a) Fabru, b) SiCeram, c) PT+A, and d) comparison of all three filament materials at 160 °C.

**Table 3**
Printing parameters for the ceramic cup.

| | SiCeram | Fabru |
|---|---|---|
| Nozzle diameter [mm] | 0.6 | 0.6 |
| Layer height [mm] | 0.2 | 0.2 |
| Extrusion width [mm] | 0.75 | 0.75 |
| Extrusion multiplier | 0.92 | 0.95 |
| Infill | 20 | 20 |
| Printing speed [mm/s] | 30 | 30 |
| Nozzle temperature [°C] | 145 | 180 |
| Printing bed temperature [°C] | 45 | 40 |
| Printing size of the cup [mm] | 77.65×85×65 | 81.7 × 89.4 × 68.4 |
| Printing time [h] | 6.5 | 6.5 |

selected feedstocks was lower as it would be expected by Fig. 7d.

The print bed temperature needed to be reduced to 40 °C to achieve sufficient adhesion. Due to the higher shrinkage of the Fabru filaments, the size of the green ceramic cup had to be printed by a factor of 1.05 larger in comparison to the SiCeram one.

After optimization of the printing parameters, ceramic cups could be printed with both filaments successfully. However, due to the significantly higher brittleness of the SiCeram filament, which was expected due to the high bending radius before fracture (see Table 1), many attempts to print a complete cup failed and it was only possible to print one complete cup structure using a 1 kg filament spool. Due to the filament brittleness, the filament broke in the printer drive wheel area and the printing process was stopped as no material was extruded. Even if manual feeding was used to recover from the print interruptions and to achieve a complete cup, breaking occurred during the solvent debinding process at the place where the process was stopped. It can be assumed that the manual adjustment during printing is risky and fusion between the layers is not sufficient.

For the Fabru filaments, this problem could not be observed because they show significantly higher flexibility. Therefore printing of several ceramic cups and other objects was possible with a 1 kg filament spool. Optical microscopy on the fracture cross-section of printed disks in the green and sintered state confirmed the absence of cracks and failures during printing and post-processing using this filament (Fig. S1).

For larger parts, Fabru GmbH recommends an additional wicking step in between the solvent and thermal debinding process. In this additional debinding step the ceramic parts are thermally debound inside a highly porous powder bed. The thermally extracted binder components will be removed from the surface of the ceramic part by capillary forces, caused by the very fine pores of the powder bed. The powder bed can significantly speed up the process as well as reduce some defects. Therefore, in Fig. 8 the printed, solvent debound, wick debound and sintered cup are presented. Fig. 9.

As shown in Fig. 8, the ceramic cup printed with SiCeram filament failed after 24 h solvent debinding. The mass loss during the different processing steps are reported in Table 4.

As shown in Fig. 2, for the Fabru YSZ filament a shrinkage of 23.7% could be observed. For the ceramic cup an outer shrinkage of 24.3% could be analysed in x-, y- and z-direction. The small difference can be explained by the measurement accuracy of the caliper used to investigate the green and sintered diameter of the YSZ filament.

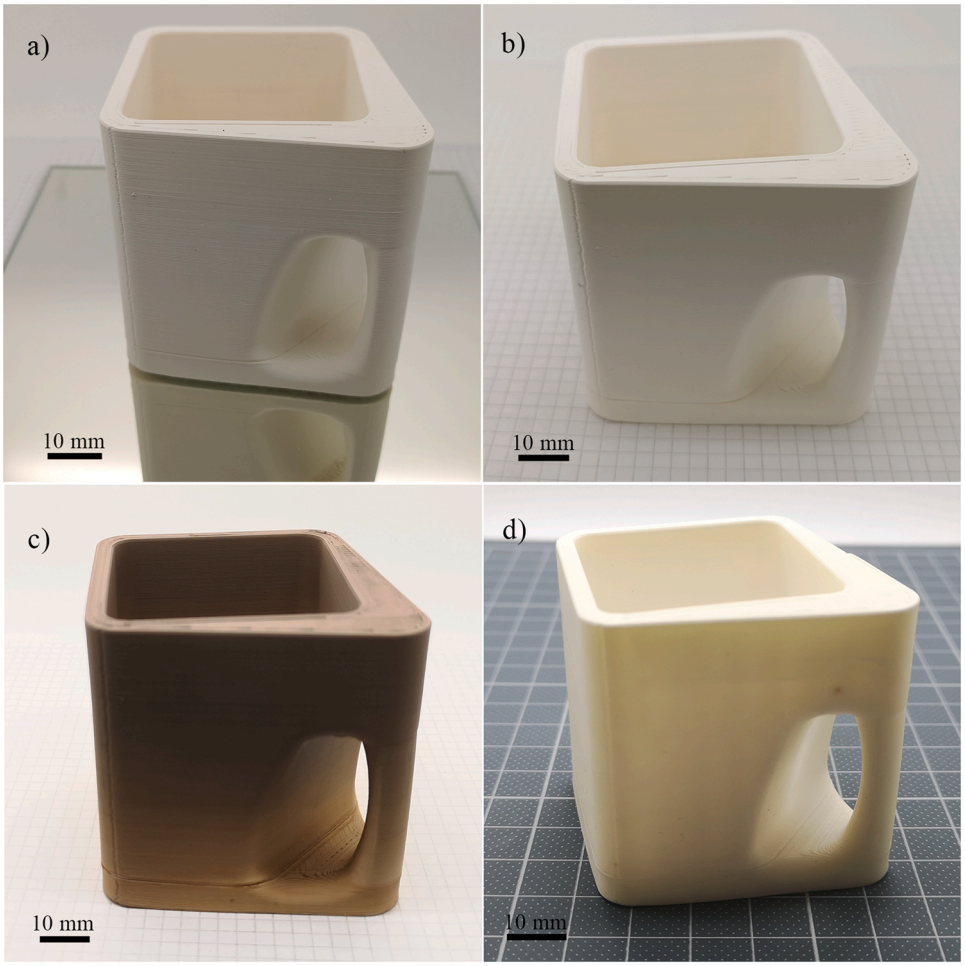


**Fig. 8.** Optical analysis of the cup printed using Fabru YSZ filament after a) printing, b) solvent debinding, c) wick debinding, and d) sintering.

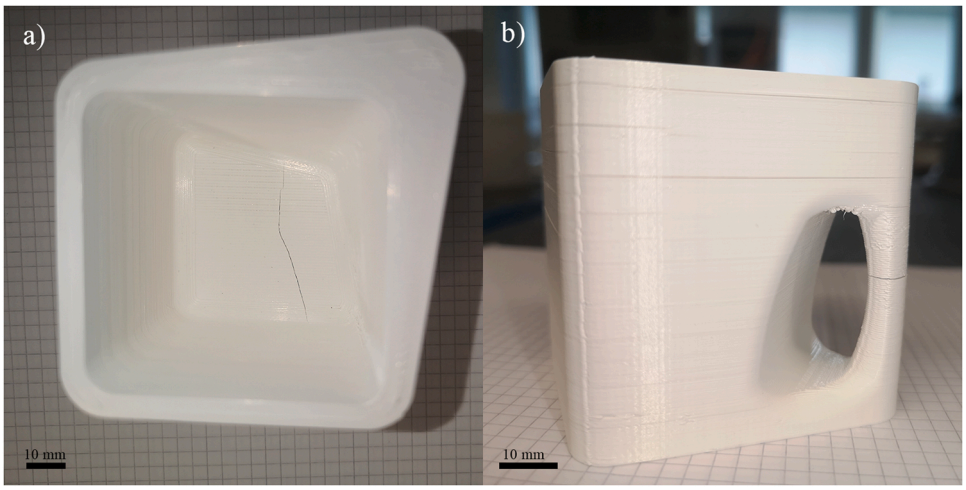


**Fig. 9.** Cup printed using SiCeram filament showing a) cracks at the bottom, and b) inter-layer cracks after solvent debinding.

**Table 4**
Mass loss and shrinkage of ceramic cups printed with selected YSZ filaments (SiCeram and Fabru).

| | SiCeram | Fabru |
|---|---|---|
| Mass loss after solvent debinding [%] | 5.4 | 6.7 |
| Mass loss after wick debinding [%] | n.a. | 2.7 |
| Total shrinkage [%] | n.a. | 24.3 |

## 4. Conclusion

In this study, we demonstrated that the analyses of further filament properties correlate with the printing parameters for the ceramic parts and the printing behavior. Even though properties like, flexibility and viscosity of the filaments are diverse, it is possible to print the same ceramic part on the same commercial printer after some parameter adjustment. Due to the rheological analysis, it can be confirmed that printing with different temperatures is needed to achieve a similar viscosity. Typically the performance of commercial print heads limits the maximal viscosity of the material that can be printed. If the viscosity is too high, printing failures like buckling and filament abrasion can be observed. Based on our results it can be assumed that viscosity data are helpful for the customer to select the right temperature if a new filament will be used.

It could be demonstrated that the printing of the ceramic cup was possible independent if the ceramic filaments are either more brittle or flexible. The main problem that was observed was the high rejection rate for the brittle filaments. This can be explained by the fracture of the filament in the drive wheel area. It was not possible to continue the printing process manually without introducing larger fusing defects that resulted in delamination during solvent debinding afterward.

In our case, the total shrinkage of the ceramic part was constant for the outer dimensions in all three directions. In our study, the total shrinkage of the ceramic part and the filament are very similar. Thereby we assume that the information about the shrinkage value of the ceramic filaments will be helpful for the customer too. However, it is worthwhile to mention that others have reported a shrinkage variation in x-, y- and z-direction due to the habitus of the ceramic powder [21], the infill orientation during printing [32] and the use of a screw extruder printing head [44].

Based on the results we advise investigating filaments before starting printing ceramic objectives. Rheology is a good tool to investigate the flow behavior of filaments to adjust the printing parameters and avoid printing failures like buckling and filament abrasion. In addition, shrinkage of the filament in x- and y-directions helps to design the geometrical size of printed structure to achieve the required values after sintering. For sure, the grain orientation in a filament will affect the properties of the final ceramic part. Therefore it is important to know such information from the beginning and it will be helpful for the customer if such information are more transparent from the filament supplier.

## Declaration of Competing Interest

The authors declare that they have no known competing financial interests or personal relationships that could have appeared to influence the work reported in this paper.

## Acknowledgments

This work was supported by the Swiss National Science Foundation (SNSF) [grant number 200021_184691/1].

## Appendix A. Supporting information

Supplementary data associated with this article can be found in the online version at doi:10.1016/j.jeurceramsoc.2022.10.019.

## References

[1] Standard, A.S.T.M., F2792. 2012. standard terminology for additive manufacturing technologies, ASTM F2792–10e1 (2012) 24.
[2] F.J. Clemens, T. Sebastian, A. Kerber, FDM/FFF an Alternative to CIM Manufacturing of Prototype and Small Quantities of Ceramic Part, Ceramic applications: components for high performance, 8 (2020) 27–31.
[3] M.K. Agarwala, R.V. Weeren, R. Vaidyanathan, A. Bandyopadhyay, G. Carrasquillo, V. Jamalabad, N. Langrana, A. Safari, S.H. Garofalini, S.C. Danforth, J. Burlew, R. Donaldson, P. Whalen, C. Ballard, Structural ceramics by fused deposition of ceramics, Int. solid freeform fabrication Symp., (1995).
[4] M.K. Agarwala, R.V. Weeren, A. Bandyopadhyay, P.J. Whalen, A. Safari, S.C. Danforth, Fused deposition of ceramics and metals: an overview, Int. solid freeform fabrication Symp., (1996).
[5] R. Clancy, V. Jamalabad, P. Whalen, P. Bhargava, C. Dai, S. Rangarajan, S. Wu, S. Danforth, N. Langrana, A. Safari, Fused deposition of ceramics: progress towards a robust and controlled process for commercialization, Int. solid freeform fabrication Symp., (1997).
[6] T.F. McNulty, F. Mohammadi, A. Bandyopadhyay, D.J. Shanefield, S.C. Danforth, A. Safari, Development of a binder formulation for fused deposition of ceramics, Rapid Prototyp. J. (1998), https://doi.org/10.1108/13552549810239012.
[7] G.M. Lous, I.A. Cornejo, T.F. McNulty, A. Safari, S.C. Danforth, Fabrication of piezoelectric ceramic/polymer composite transducers using fused deposition of ceramics, J. Am. Ceram. Soc. 83 (2000) 124–128, https://doi.org/10.1111/j.1151-2916.2000.tb01159.x.
[8] N. Venkataraman, S. Rangarajan, M.J. Matthewson, B. Harper, A. Safari, S. C. Danforth, A. Yardimci, Feedstock material property–process relationships in fused deposition of ceramics (FDC), Rapid Prototyp. J. 6 (2000) 244–253, https://doi.org/10.1108/13552540010373344.

[9] S. Rangarajan, G. Qi, N. Venkataraman, A. Safari, S.C. Danforth, Powder processing, rheology, and mechanical properties of feedstock for fused deposition of Si3N4, Ceram., J. Am. Ceram. Soc. 83 (2000) 1663–1669, https://doi.org/10.1111/j.1151-2916.2000.tb01446.x.
[10] M.A. Jafari, W. Han, F. Mohammadi, A. Safari, S.C. Danforth, N.J.R.P.J. Langrana, A novel system for fused deposition of advanced multiple ceramics, Rapid Prototyp. J. (2000), https://doi.org/10.1108/13552540010337047.
[11] M. Allahverdi, S.C. Danforth, M. Jafari, A. Safari, Processing of advanced electroceramic components by fused deposition technique, J. Eur. Ceram. Soc. 21 (2001) 1485–1490, https://doi.org/10.1016/S0955-2219(01)00047-4.
[12] M.M. Bach, T. Sebastian, M. Melnykowycz, T. Lusiola, D. Scharf, F. Clemens, Additive Manufacturing of Piezoelectric 3–3 Composite Structures, International Conference on Additive Manufacturing in Products and Applications, Springer, Cham., (2017) 93–103. https://doi.org/10.1007/978–3-319–66866-6_9.
[13] M. Janek, V. Žilinská, V. Kovár, Z. Hajdúchová, K. Tomanová, P. Peciar, P. Veteška, T. Gabošová, R. Fialka, J. Feranc, L. Omaníková, R. Plavec, Ľ. Bača, Mechanical testing of hydroxyapatite filaments for tissue scaffolds preparation by fused deposition of ceramics, J. Eur. Ceram. Soc. 40 (2020) 4932–4938, https://doi.org/10.1016/j.jeurceramsoc.2020.01.061.
[14] A. Bellini, L. Shor, S.I. Guceri, New developments in fused deposition modeling of ceramics, Rapid Prototyp. J. (2005), https://doi.org/10.1108/13552540510612901.
[15] C. Lieberwirth, M. Sarhan, H. Seitz, Mechanical properties of stainless-steel structures fabricated by composite extrusion modelling, Metals 8 (2018) 84, https://doi.org/10.3390/met8020084.
[16] W. Kollenberg, D. Nikolay, Additive fertigung keramischer bauteile, Keram. Z. 70 (2018) 22–25, https://doi.org/10.1007/s42410-018-0008-9.
[17] H. Giberti, M. Strano, M. Annoni, An innovative machine for Fused Deposition Modeling of metals and advanced ceramics, MATEC Web Conf., 43 (2016) 03003. https://doi.org/10.1051/matecconf/20164303003.
[18] Q. He, J. Jiang, X. Yang, L. Zhang, Z. Zhou, Y. Zhong, Z. Shen, Additive manufacturing of dense zirconia ceramics by fused deposition modeling via screw extrusion, J. Eur. Ceram. Soc. 41 (2021) 1033–1040, https://doi.org/10.1016/j.jeurceramsoc.2020.09.018.
[19] H. Masuda, Y. Ohta, M. Kitayama, Additive manufacturing of SiC ceramics with complicated shapes using the FDM type 3D-printer, J. Mater. Sci. Chem. Eng. 7 (2019) 1, https://doi.org/10.4236/msce.2019.72001.
[20] F. Clemens, J. Schulz, L. Gorjan, A. Liersch, T. Sebastian, F. Sarraf, Debinding and Sintering of Dense Ceramic Structures Made with Fused Deposition Modeling, Int. Conf. on Additive Manufacturing in Products and Applications, Springer, Cham, (2020) 293–303. https://doi.org/10.1007/978–3-030–54334-1_21.
[21] N.A. Conzelmann, L. Gorjan, F. Sarraf, L.D. Poulikakos, M.N. Partl, C.R. Müller, F. J. Clemens, Manufacturing complex Al2O3 ceramic structures using consumer-grade fused deposition modelling printers, Rapid Prototyp. J. 26 (2020) 1035–1048, https://doi.org/10.1108/RPJ-05-2019-0133.
[22] F. Sarraf, E. Abbatinali, L. Gorjan, T. Sebastian, P. Colombo, S.V. Churakov, F. J. Clemens, Effect of MgO sintering additive on mullite structures manufactured by fused deposition modeling (FDM) technology, J. Eur. Ceram. Soc. 41 (2021) 6677–6686, https://doi.org/10.1016/j.jeurceramsoc.2021.06.012.
[23] Q. He, J. Jiang, X. Yang, L. Zhang, Z. Zhou, Y. Zhong, Z. Shen, Additive manufacturing of dense zirconia ceramics by fused deposition modeling via screw extrusion, J. Eur. Ceram. Soc. 41 (2021) 1033–1040, https://doi.org/10.1016/j.jeurceramsoc.2020.09.018.
[24] J. Abel, U. Scheithauer, T. Janics, S. Hampel, S. Cano, A. Müller-Köhn, A. Günther, C. Kukla, T. Moritz, Fused Filament Fabrication (FFF) of metal-ceramic components, JoVE (J. Vis. Exp. ) 143 (2019) 57693, https://doi.org/10.3791/57693.
[25] D. Nötzel, R. Eickhoff, T. Hanemann, Fused filament fabrication of small ceramic components, Materials 11 (2018) 1463, https://doi.org/10.3390/ma11081463.
[26] S. Cano, J. Gonzalez-Gutierrez, J. Sapkota, M. Spoerk, F. Arbeiter, S. Schuschnigg, F. Arbeiter, S. Schuschnigg, C. Kukla, Additive manufacturing of zirconia parts by fused filament fabrication and solvent debinding: Selection of binder formulation, Addit. Manuf. 26 (2019) 117–128, https://doi.org/10.1016/j.addma.2019.01.001.
[27] J.M. Bauer, R. Seemann, N.M. Durakbasa, M. Lackner, Fused Filament Fabrication of Ceramic Components for Home Use, Digital Conversion on the Way to Industry 4.0: Selected Papers from ISPR2020, September 24–26, 2020 Online-Turkey, 121 (2020). https://doi.org/10.1007/978–3-030–62784-3_11.
[28] M. Orlovská, Z. Chlup, Ľ. Bača, M. Janek, M. Kitzmantel, Fracture and mechanical properties of lightweight alumina ceramics prepared by fused filament fabrication, J. Eur. Ceram. Soc. 40 (2020) 4837–4843, https://doi.org/10.1016/j.jeurceramsoc.2020.02.026.
[29] D. Nötzel, T. Hanemann, New feedstock system for fused filament fabrication of sintered alumina parts, Materials 13 (2020) 4461, https://doi.org/10.3390/ma13194461.
[30] K. Sudan, P. Singh, A. Gökçe, V.K. Balla, K.H. Kate, Processing of hydroxyapatite and its composites using ceramic fused filament fabrication (CF3, Ceram. Int. 46 (2020) 23922–23931, https://doi.org/10.1016/j.ceramint.2020.06.168.
[31] L. Gorjan, C. Galusca, M. Sami, T. Sebastian, F. Clemens, Effect of stearic acid on rheological properties and printability of ethylene vinyl acetate based feedstocks for fused filament fabrication of alumina, Addit. Manuf. 36 (2020), 101391, https://doi.org/10.1016/j.addma.2020.101391.
[32] S. Cano, T. Lube, P. Huber, A. Gallego, J.A. Naranjo, C. Berges, S. Schuschnigg, G. Herranz, C. Kukla, C. Holzer, J. Gonzalez-Gutierrez, Influence of the infill orientation on the properties of zirconia parts produced by fused filament fabrication, Materials 13 (2020) 3158, https://doi.org/10.3390/ma13143158.
[33] A.C. Marsh, Y. Zhang, L. Poli, N. Hammer, A. Roch, M. Crimp, X. Chatzistavrou, 3D printed bioactive and antibacterial silicate glass-ceramic scaffold by fused filament fabrication, Mater. Sci. Eng.: C. 118 (2021), 111516, https://doi.org/10.1016/j.msec.2020.111516.
[34] C. Berges, A. Wain, R. Andújar, J.A. Naranjo, A. Gallego, E. Nieto, G. Herranz, R. Campana, Fused filament fabrication for anode supported SOFC development: towards advanced, scalable and cost-competitive energetic systems, Int. J. Hydrog. Energy 46 (2021) 26174–26184, https://doi.org/10.1016/j.ijhydene.2021.02.097.
[35] U. Lohse, Fused filament fabrication of ceramic components, Inter. Int. Ceram. Rev. 70 (2021) 22–27, https://doi.org/10.1007/s42411-021-0470-z.
[36] W. Freudenberg, F. Wich, N. Langhof, S. Schafföner, Additive manufacturing of carbon fiber reinforced ceramic matrix composites based on fused filament fabrication, J. Eur. Ceram. Soc. 42 (2022) 1822–1828, https://doi.org/10.1016/j.jeurceramsoc.2021.12.005.
[37] J. Abel, W. Kunz, A. Michaelis, M. Singh, H. Klemm, Non-oxide CMC fabricated by fused filament fabrication (FFF), Int. J. Appl. Ceram. 19 (2022) 1148–1155, https://doi.org/10.1111/ijac.13944.
[38] K. Rane, M. Strano, A comprehensive review of extrusion-based additive manufacturing processes for rapid production of metallic and ceramic parts, Adv. Manuf. 7 (2019) 155–173, https://doi.org/10.1007/s40436-019-00253-6.
[39] T. Sebastian, M. Bach, A. Geiger, T. Lusiola, L. Kozielski, F. Clemens, Investigation of electromechanical properties on 3-D printed piezoelectric composite scaffold structures, Materials 14 (2021) 5927, https://doi.org/10.3390/ma14205927.
[40] A. Hadian, L. Koch, P. Koberg, F. Sarraf, A. Liersch, T. Sebastian, F. Clemens, Material extrusion based additive manufacturing of large zirconia structures using filaments with ethylene vinyl acetate based binder composition, Addit. Manuf. 47 (2021), 102227, https://doi.org/10.1016/j.addma.2021.102227.
[41] M. Mader, L. Hambitzer, P. Schlautmann, S. Jenne, C. Greiner, F. Hirth, D. Helmer, F. Kotz-Helmer, B.E. Rapp, Melt-extrusion-based additive manufacturing of transparent fused silica glass, Adv. Sci. 8 (2021), 2103180, https://doi.org/10.1002/advs.202103180.
[42] W. Li, A. Armani, A. Martin, B. Kroehler, A. Henderson, T. Huang, J. Watts, G. Hilmas, M. Leu, Extrusion-based additive manufacturing of functionally graded ceramics, J. Eur. Ceram. Soc. 41 (2021) 2049–2057, https://doi.org/10.1016/j.jeurceramsoc.2020.10.029.
[43] K. Rane, M.A. Farid, W. Hassan, M. Strano, Effect of printing parameters on mechanical properties of extrusion-based additively manufactured ceramic parts, Ceram. Int. 47 (2021) 12189–12198, https://doi.org/10.1016/j.ceramint.2021.01.066.
[44] A. Hadian, M. Fricke, A. Liersch, F. Clemens, Material extrusion additive manufacturing of zirconia parts using powder injection molding feedstock compositions, Addit. Manuf. (2022), 102966, https://doi.org/10.1016/j.addma.2022.102966.
[45] X.J. Yang, C. Pin, A.G. Fane, Separation of hafnium from zirconium by extraction chromatog-raphy with liquid anionic exchangers, J. Chromatogr. Sci. 37.5 (1999) 171–179, https://doi.org/10.1093/chromsci/37.5.171.
[46] C. Gross, T. Bergfeldt, T. Fretwurst, R. Rothweiler, K. Nelson, A. Stricker, Elemental analysis of commercial zirconia dental implants-Is “metal-free” devoid of metals? J. Mech. Behav. Biomed. Mater. 107 (2020), 103759 https://doi.org/10.1016/j.jmbbm.2020.103759.